# Relativistic electron microbursts associated with whistler chorus rising tone elements: GEMSIS-RBW simulations

S. Saito,[1] Y. Miyoshi,[2] and K. Seki[2,3]

Received 11 June 2012; revised 29 August 2012; accepted 4 September 2012; published 6 October 2012.

[1] Relativistic electron microbursts, which are bursty enhancements of the precipitation of relativistic electrons, are often observed by low-altitude satellite measurements. These microbursts are likely to play an important role in high-energy electron flux loss in the outer radiation belt. Some observations suggest that whistler chorus waves are a cause of relativistic electron microbursts. First, we derived the relativistic time of flight model considering the propagation of whistler mode waves, and then investigated characteristics of the precipitations. We found that relativistic electron precipitation has a positive energy dispersion at low altitude. The duration of electron precipitation by one whistler chorus element decreases when the energy of the precipitated electrons is increased. We then performed three-dimensional test particle simulation with a newly developed wave-particle interaction model using realistic plasma parameters in the inner magnetosphere. The test particle simulation showed for the first time that the resonant interactions with whistler chorus elements at high-latitudes produce bursty enhancements of relativistic electron precipitation, thus confirming the results of the TOF analysis. A few Hz modulations are embedded in the precipitating electron flux variations, which is associated with the repetition period of the whistler chorus elements. The simulation results indicate that microbursts of relativistic electrons of the outer belt are caused by chorus wave-particle interactions at high latitudes and a series of rising tone elements of chorus waves produce a few Hz modulation of microbursts observed by the SAMPEX satellite.

**Citation:** Saito, S., Y. Miyoshi, and K. Seki (2012), Relativistic electron microbursts associated with whistler chorus rising tone elements: GEMSIS-RBW simulations, *J. Geophys. Res.*, *117*, A10206, doi:10.1029/2012JA018020.

## 1. Introduction

[2] Relativistic electron microbursts are the bursty precipitation of relativistic electrons into the atmosphere within one second [e.g., *Nakamura et al.*, 1995, 2000; *Millan et al.*, 2002; *O'Brien et al.*, 2004], that can sometimes occur with multiple bursts [*Lorentzen et al.*, 2001a]. These bursts are likely to play an important role in the loss of relativistic electrons in the outer radiation belt [*Lorentzen et al.*, 2001b].

[3] Some mechanisms have been proposed as a cause of the relativistic electron precipitation [see *Millan and Thorne*, 2007; *Ebihara and Miyoshi*, 2011; *Turner et al.*, 2012]. One contributor is thought to be the electromagnetic ion cyclotron (EMIC) wave. *Thorne and Kennel* [1971] suggested that the EMIC wave can scatter relativistic electrons thorough wave-particle interactions. *Summers and Thorne* [2003] and *Albert* [2003] calculated relativistic electron pitch angle diffusion rates for EMIC waves in a multi-ion plasma. Their results suggest that the EMIC waves with typical wave amplitudes (1–10 nT) can lead to intense relativistic electron precipitation. This scattering process removes energetic electrons (>1 MeV) from the outer radiation belt during a magnetic storm over a time scale of one day. *Bortnik et al.* [2006] analyzed data from a relativistic electron dropout event showing precipitation of relativistic electrons and energetic protons at low L shells (<5). They found that the precipitation can be explained by the pitch angle scattering driven by EMIC waves. *Jordanova et al.* [2008] simulated a kinetic ring current-atmosphere interactions model (RAM) including EMIC-relativistic electrons interacting self-consistently and found that EMIC waves actually cause the precipitation loss of MeV electrons. *Miyoshi et al.* [2008] have given observational evidence from satellite and ground-based data that EMIC waves cause simultaneous precipitation of ring current ions and MeV electrons of the outer radiation belt.

[4] Another contributor is thought to be whistler waves, i.e., the whistler chorus and the hiss in the inner magnetosphere. *Horne and Thorne* [2003] and *Thorne et al.* [2005] discussed the importance of off-equatorial scattering of relativistic electrons near the magnetic loss cone angle, which can precipitate them through the first-order electron cyclotron

[1]National Institute of Information and Communications Technology, Tokyo, Japan.
[2]Solar-Terrestrial Environment Laboratory, Nagoya University, Nagoya, Japan.
[3]Institute for Advanced Research, Nagoya University, Nagoya, Japan.

Corresponding author: S. Saito, National Institute of Information and Communications Technology, 4-2-1 Nukui-Kitamachi, Koganei, Tokyo 184-8795, Japan. (ssaito@nict.go.jp)


0148-0227/12/2012JA018020

resonance. *Lorentzen et al.* [2001a] found that relativistic electron microbursts (>1 MeV) were accompanied with a group of lower band whistler chorus consisting of several discrete elements with a rising tone of frequency typically between 0.1 $|\Omega_e|$ and 0.4 $|\Omega_e|$, where $|\Omega_e|$ is an electron cyclotron frequency at the equator. These discrete chorus emissions are typically repeated with a few hundred msec periods. The period of discrete chorus emissions seems to be close to that of the flux variation of relativistic electron microbursts observed by the SAMPEX satellite [*Nakamura et al.*, 1995], where the few Hz modulation of the microbursts is associated with the bounce time of the relativistic electrons. Occurrence of relativistic electron microbursts during magnetic storms depends on magnetic local time, which increases mainly in the dawn sector [*Nakamura et al.*, 2000; *O'Brien et al.*, 2003; *Johnston and Anderson*, 2010]. The whistler chorus emission tends to be active in the dawn sector [e.g., *Li et al.* 2009], while the EMIC waves tend to be generated in the dusk and midnight sectors during magnetic storms [e.g., *Jordanova et al.*, 2008, 2010]. Considering these characteristics, it seems reasonable that the most plausible contributor to relativistic electron microbursts in the dawnside is whistler chorus waves. However, as yet there is no clear evidence to definitively identify the cause of the relativistic electron microbursts.

[5] The microphysics of wave-particle interaction between whistler waves and electrons around the equator of the dipole magnetic field has been demonstrated. Using a test-particle simulation, *Omura et al.* [2007] demonstrated relativistic turning acceleration (RTA) that accelerates electrons with keV to MeV energy around the equator of the dipole magnetic field. Whistler waves with a constant frequency effectively accelerate the electrons near a pitch angle of 90°. Using the same method, *Furuya et al.* [2008] confirmed that the RTA in a rising tone of whistler chorus can be applied at the equator. Their simulations suggest that significant acceleration and scattering take place in a very short timescale, which cannot be described in a quasi-linear diffusion theory.

[6] *Katoh and Omura* [2007] have performed self-consistent electron hybrid simulations for whistler chorus generation and RTA. They showed that energetic electrons scattered by the whistler chorus in the dipole field are accelerated around the equatorial pitch angle of 90°, as also discussed in *Omura et al.* [2007]. *Hikishima et al.* [2010] demonstrated the microburst precipitation of non-relativistic (tens-keV) electrons associated with whistler chorus emissions in the dipole magnetic field through self-consistent full kinetic particle-in-cell simulations. Their results revealed that the precipitation of tens-keV electrons is bursty-enhanced when the whistler chorus is generated. The energy dispersion of the precipitated electrons seen in this simulation was negative: that is, low-energy electron precipitations were observed following the high-energy electron precipitations. While keV electrons near the loss cone angle can resonate with the whistler chorus under the first-order cyclotron resonance condition, relativistic electrons near the loss cone cannot satisfy this condition around the equator. Thus, scattering at relatively high magnetic latitudes is required [*Horne and Thorne*, 2003] to precipitate the relativistic electrons.

[7] In this study, we focus on the microphysics of wave-particle interaction and consider chorus waves propagating along the field line to high magnetic latitudes from the magnetic equator. To demonstrate wave-particle interactions at the off-equatorial region in the inner magnetosphere, we developed the Geospace Environment Modeling System for Integrated Studies – Radiation Belt with Wave-particle interaction module (GEMSIS-RBW) simulation code, which is a modification of the GEMSIS-Radiation Belt (RB) code [*Saito et al.*, 2010].

[8] The rest of this paper is organized as follows. In section 2, we describe the time-of-flight (TOF) model of scattered electrons considering the propagation of the whistler waves along the field line of the dipole field model. In section 3, we briefly describe the GEMSIS-RBW model. The simulation model and parameters are shown in section 4. The GEMSIS-RBW simulation results in section 5 show that relativistic electrons are precipitated into the atmosphere and have precipitation synchronized with whistler chorus emission with significant time delay. In these simulations, we identified frequency modulations of the count rate of the precipitated electrons. In the final section, we summarize our results.

## 2. Time of Flight Model

[9] We consider the time of flight (TOF) of scattered electrons near the loss cone angle, including relativistic regime, following the non-relativistic TOF model in the dipole magnetic field [*Miyoshi et al.*, 2010]. In this model, the wave-particle interactions occur along the field line on which whistler waves propagate to high magnetic latitudes. We assume the first-order resonance condition

$$\omega - \mathrm{k}_{\parallel} \mathrm{v}_{\parallel,e} = \frac{|\Omega_e|}{\gamma_e} \tag{1}$$

for the electron scattering by whistler wave propagating parallel to the dipole magnetic field line. Here $\omega$, $\mathrm{k}_{\parallel}$, $\mathrm{v}_{\parallel,e}$, $\Omega_e$, and $\gamma_e$ are angular wave frequency, parallel wave number, parallel speed of the electron, electron cyclotron angular frequency $q_eB/m_e$, and electron relativistic Lorentz gamma $\sqrt{1 + p_e^2/(m_e^2c^2)}$, respectively. Quantities $q_e$, $m_e$, $p_e$, $B$, and $c$ are electron charge, mass, momentum, the magnetic field strength at the electron position, and the speed of light.

[10] Under the cold plasma approximation, the wave number of whistler waves propagating parallel to the magnetic field line is

$$k_{\parallel} = \frac{\omega}{c}\sqrt{1 + \frac{\omega_e^2}{\omega(|\Omega_e| - \omega)}}, \tag{2}$$

where $\omega_e$ is the electron plasma frequency. The loss cone angle at the equator is evaluated as $\alpha_{lc} = \sin^{-1}\sqrt{B/B_a}$. Here, $\mathrm{B}_a$ is the field intensity at the atmospheric altitude (~100 km). The parallel speed of electrons with the loss cone pitch angle $\alpha_{\mathrm{lc}}$ is $v_{\parallel,lc} = p_e\cos\alpha_{lc}/m_e\gamma_e$, thus,

$$v_{\parallel,lc}^2 = \frac{p_e^2}{m_e^2\gamma_e^2}\left(1 - \frac{B}{B_a}\right) \tag{3}$$

Assuming the frequency of the whistler wave is constant during propagation along the magnetic field line, equations (1)–(3) derive the magnetic field intensity at the colatitude

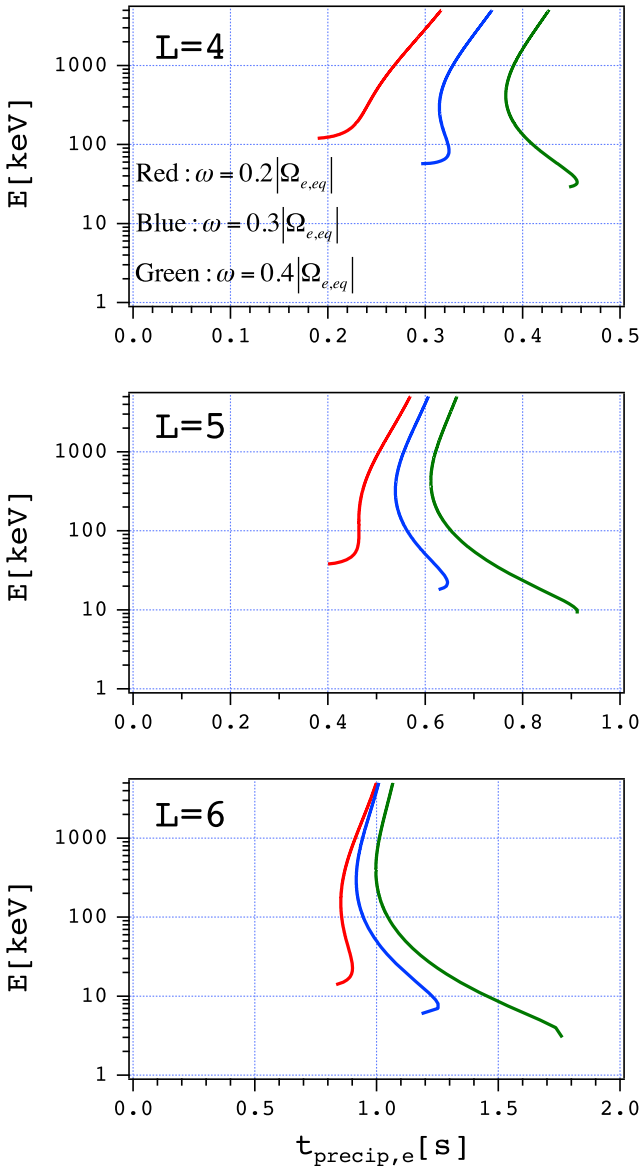


**Figure 1.** Kinetic energy of precipitated electrons as a function of the precipitation time at $L$ = 4, 5, and 6 in the dipole magnetic field. Electrons are scattered by whistler waves with $\omega$ = 0.2 (red), 0.3 (blue), and 0.4 $|\Omega_{e,eq}|$ (green).

$\theta_{res}$, where the electron satisfies the resonance condition with the whistler wave propagating in the opposite direction to the electrons.

[11] Here, we consider the whistler wave that propagates from the equator ($\theta$ = 90°) to $\theta_{res}$ in the northern (southern) hemisphere in the dipole magnetic field. The scattered electrons at $\theta_{res}$ in the northern (southern) hemisphere precipitate into the atmosphere in the southern (northern) hemisphere. Here, we define the precipitation time of an electron as

$$t_{precip,e} = t_{tr,w} + t_{tr,e} + 0.25t_b + t_L. \quad (4)$$

Quantities $t_{tr,w}$, $t_{tr,e}$, $t_b$, and $t_L$ are the transit time of whistler wave, the transit time of scattered electrons, the electron bounce time, and the launch time of whistler wave, respectively. The transit time of whistler wave propagating from the equator to the colatitude $\theta_{res}$ in the dipole field model is

$$t_{tr,w} = \int_{s=0}^{s_{res}} v_g^{-1} ds = \int_{\pi/2}^{\theta_{res}} v_g^{-1} R_0 \left(1 + 3\cos^2\theta\right)^{1/2} \sin\theta d\theta, \quad (5)$$

where $v_g$ is the group velocity of parallel propagating whistler wave, $S$ is the distance from the equator along the magnetic field line, and $S_{res}$ is the distance at the resonance point on the field line. The transit time of scattered electrons at the loss cone pitch angle from the resonant point to the equator is

$$t_{tr,e} = \int_{s=s_{res}}^{0} |v_{\parallel,lc}|^{-1} ds = \int_{\theta_{res}}^{\pi/2} |v_{\parallel,lc}|^{-1} R_0 \left(1 + 3\cos^2\theta\right)^{1/2} \sin\theta d\theta. \quad (6)$$

The third term of equation (4) is a quarter of the bounce time $t_b$ of electron near the loss cone, which is defined as the transit time of an electron moving from the equator to the atmosphere. An approximated formula of $t_b$ [*Walt*, 1994] is

$$t_b = 0.117 \frac{R_0 c}{R_E v_{\parallel,e}} \left(1 - 0.4635 \left(\sin\alpha_{eq}\right)^{3/4}\right). \quad (7)$$

When the whistler wave is launched at the equator at $t = t_L$, the counter-moving electrons with the whistler can resonate at $\theta_{res}$ at $t = t_{tr,w} + t_L$. If the electrons are scattered into the loss cone at $\theta_{res}$, they are precipitated into the atmosphere in the opposite hemisphere. The scattered electron reaches the equator at $t = t_{tr,e} + t_{tr,w} + t_L$. After that, the electron takes a quarter of $t_b$ to reach the atmosphere.

[12] Figure 1 shows the electron kinetic energy as a function of the precipitation time of electrons at $L$ = 4, 5, and 6 in the dipole magnetic field model. Precipitated electrons resonate with whistler waves with $\omega$ = 0.2, 0.3, and 0.4 $|\Omega_{e,eq}|$, which are shown as red, blue, and green, respectively. Here $\Omega_{e,eq}$ is the electron cyclotron angular frequency at the equator where whistler chorus elements are launched. The launch time $t_L$ is related to frequency drift rate $d\omega/dt = 2|\Omega_{e,eq}|$ rad/$s^2$. This rate means that $\omega$ increases $0.2|\Omega_{e,eq}|$ rad/s during 100 msec, which is similar to the frequency drift of the raising tone of whistler chorus observed by Cluster [e.g., *Santolík et al.*, 2003]. In this case, $t_L(\omega = 0.4|\Omega_{e,eq}|) = t_L(\omega = 0.2|\Omega_{e,eq}|) + 100$ msec. Here, we assume $t_L(\omega = 0.2|\Omega_{e,eq}|) = 0$ and constant electron plasma frequency $\omega_e \sim 180 \times 10^3$ rad/s in space. The whistler waves propagate to high magnetic latitudes, and scatter relativistic electrons near the loss cone pitch angle. As shown in Figure 1, at non-relativistic energies (<a few tens keV), the energy dispersion tends to be negative. In contrast, at relativistic energies >500 keV, the energy dispersion becomes positive. The sign of the energy dispersion changes between 100 keV and 1 MeV and is significant at higher $L$ values and higher resonant frequencies. At $L$ = 4, the energy dispersion of electrons scattered by $\omega = 0.2|\Omega_{e,eq}|$ has only the positive sign.

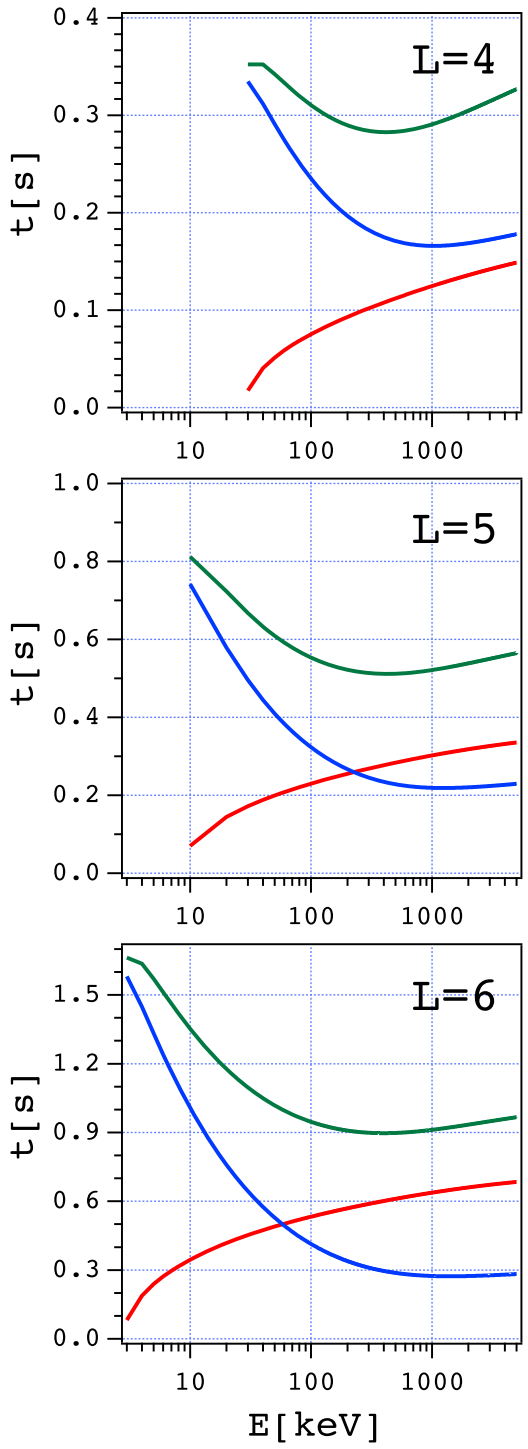


**Figure 2.** The transit time of whistler wave (solid red: $t_{tr,w}$), the TOF of electrons (solid blue: $t_{tr,e} + 0.25\ t_b$), and electron precipitation time (solid green: $t_{precip,e}$) are shown as a function of kinetic energy of electrons scattered by whistler wave with $\omega = 0.4\ |\Omega_{e,eq}|$ on (top) $L = 4$, (middle) 5, and (bottom) 6.

[13] The energy dependence of the precipitation time is described by the transit time of whistler wave ($t_{tr,w}$) and the electron flight time ($t_{tr,e} + 0.25\ t_b$). Figure 2 shows the transit time of whistler waves (solid red: $t_{tr,w}$), the traveling time of electrons (solid blue: $t_{tr,e} + 0.25t_b$), and the electron precipitation time (solid green: $t_{precip,e}$) as a function of kinetic energy of the electrons scattered by whistler wave with $\omega = 0.4\ |\Omega_{e,eq}|$ on $L = 4$ (top), 5 (middle), and 6 (bottom). The energy dependence of $t_{tr,w}$ is the result of differences of $\theta_{res}$. At non-relativistic energies, the energy dispersion is dominant in the electron precipitation time, supporting the idea that negative dispersion is due to the TOF effect, as described in *Miyoshi et al.* [2010]. The scattered electrons at higher energies overtake the electrons at lower energies before reaching the atmosphere. At relativistic energies, the time of flight is almost independent of the energy, while the whistler transit time gradually increases. In this energy range, the flight speed of electrons is close to the speed of light, so the flight time tends to be independent of energy. This indicates that the positive energy dispersion seen in Figure 1 is due to the whistler transit time gradually increasing in energy. The whistler transit time increases when the scattered electron energy increases because the higher-energy electrons are scattered at higher magnetic latitudes where the frequency ratio $\omega/|\Omega_e|$ becomes smaller.

[14] Figure 3 shows the estimated duration of electron precipitation associated with one whistler chorus element at $L$ = 4, 5, and 6. Duration $\Delta T$ is defined as

$$\Delta T(E) = t_{precip,e}(E, \omega = \omega_{\max}) - t_{precip,e}(E, \omega = \omega_{\min}). \quad (8)$$

Note that higher frequency components of the rising tone chorus are launched later at the equator, and therefore the electrons scattered by higher frequency whistler waves are precipitated later. The duration of electron precipitation decreases when the energy increases (Figure 3), which is a trend seen in both non-relativistic and relativistic regimes.

## 3. GEMSIS-RBW Code

[15] Geospace Environment Modeling System for Integrated Studies – Radiation Belt with Wave-particle interaction (GEMSIS-RBW) simulation code is the GEMSIS-RB simulation code [*Saito et al.*, 2010] with the Wave-Particle Interaction (WPI) model. The GEMSIS-RB is a relativistic test particle code in three-dimensional electromagnetic

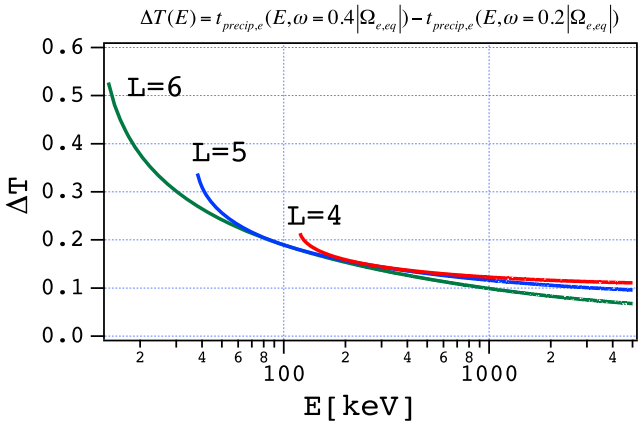


**Figure 3.** Intervals between $t_{precip,e}(E,\ \omega = 0.2\ |\Omega_{e,eq}|)$ and $t_{precip,e}(E,\ \omega = 0.4\ |\Omega_{e,eq}|)$ as a function of kinetic energy of precipitated electrons, which are plotted at $L$ = 4 (red), 5 (blue), and 6 (green).

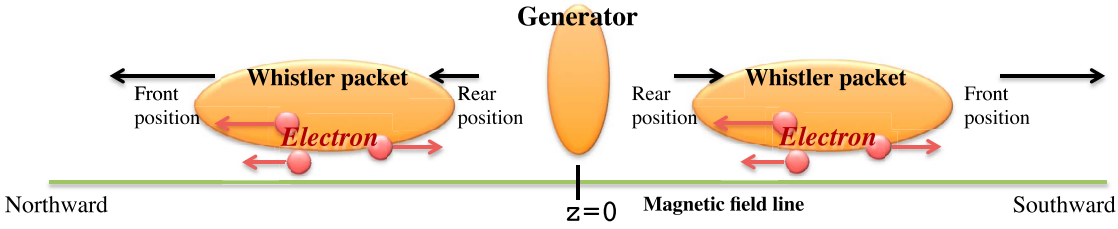


**Figure 4.** Overview of the WPI model shows parallel propagation of whistler wave packets and electron scattering. Wave packets are generated at the magnetic equator and propagate in both northern and southern directions.

fields, which solves the guiding center equations derived by *Brizard and Chan* [1999]. This calculates electron parallel and perpendicular momentum $p_{\parallel}$ and $p_{\perp}$, as well as guiding center position $\boldsymbol{R}$, while the WPI simulation solves the equation of motion for the electron momentum change.

[16] Figure 4 shows the basic concept of the WPI model. This model demonstrates parallel propagation of whistler wave packets and electron scattering. The wave packets are generated at the magnetic equator and propagate in both the northern and southern directions along the field line with its group velocity $v_g$. The wave packets contain wave information, such as frequency, wave number, and amplitude. Here we use the spatial coordinate system ($L^*$, MLT, $s$) for the wave propagation in the dipole magnetic field where $L^*$, MLT, and $s$ are Roederer-$L$ shell [*Roederer*, 1970], local time, and distance from the magnetic equator along the field line, respectively. We assume the whistler waves propagate only in the parallel direction, thus the wave packet changes only $s$ in this coordinate system. When the wave packet interacts with electrons bouncing along the magnetic field, the WPI module calculates electron momentum changes during $\Delta t$, where $\Delta t$ is the time step of the GEMSIS-RB model.

[17] The electron momentum changes are calculated using the following equation of motion:

$$\frac{d}{dt}\mathbf{p}_e = q_e(\delta\mathbf{E} - \mathbf{v}_e \times (\mathbf{B} + \delta\mathbf{B})), \tag{9}$$

where $\mathbf{v}_e = \mathbf{p}_e/m_e\gamma_e$ is the electron velocity and $\mathbf{B}$ is the background magnetic field vector. The initial gyrophase of an electron in the WPI model is randomly chosen when the electron collides with chorus elements. $\delta\mathbf{E}$ and $\delta\mathbf{B}$ are vectors of electric and magnetic field fluctuations, respectively, and they satisfy the dispersion relation of the whistler mode waves.

[18] The electromagnetic fluctuations at the electron position are defined as

$$\delta\mathbf{B} = \left(\delta B_{\perp}, \delta B_{\perp\perp}, \delta B_{\parallel}\right) = (\delta B\cos\phi, -\delta B\sin\phi, 0) \tag{10}$$

$$\delta\mathbf{E} = \left(\delta E_{\perp}, \delta E_{\perp\perp}, \delta E_{\parallel}\right) = (-\delta E\sin\phi, -\delta E\cos\phi, 0) \tag{11}$$

Subscripts $\parallel$, $\perp$, and $\perp\perp$ indicate the parallel, perpendicular, and other perpendicular directions of the background magnetic field $\mathbf{B}$. Quantity $\varphi$ shows wave-phase of whistler waves at the electron position. Note that directions $\perp$ and $\perp\perp$ are defined by $\varphi$ for each electron. Assuming wave parameters at the electron position are constant during $\Delta t$, the wave phase $\varphi$ during $\Delta t$ is

$$\phi^{t+\delta t} = k_{\parallel}\mathrm{v}_{\parallel}\delta t - \omega\delta t + \phi^{t}. \tag{12}$$

The superscript $t$ of $\varphi$ denotes time. The equation of motion is numerically solved with the time step $\delta t = 2\pi\Omega_e^{-1}X^{-1}$ during $\Delta t$, where we choose $X \sim 30$ to resolve the cyclotron motion. After the calculation in $\Delta t$, the first adiabatic invariant of the electron at $t + \Delta t$ is calculated using the background magnetic field intensity at the electron position. After scattering, the electron position is advanced through the GEMSIS-RB model. Under this method, GEMSIS-RB model calculates electron motion that keeps the first adiabatic invariant in electromagnetic fields, while WPI model breaks the invariants when the electrons interact with whistler waves. When the electron cyclotron resonance condition is satisfied during the interaction, the first and second adiabatic invariants are broken, meaning electron scattering occurs in pitch angle and energy.

## 4. Simulation Model

[19] We demonstrate relativistic electron precipitation scattered by rising tone elements of whistler chorus propagating to high magnetic latitudes (~40° where whistler waves can scatter electrons with energy larger than a few MeV) at $L^* = 6$ in the dipole magnetic field by using GEMSIS-RBW simulations. Each chorus element has a frequency drift between 0.2 $|\Omega_{e,eq}|$ and 0.43 $|\Omega_{e,eq}|$ during ~120 msec on the magnetic equator (as shown in Figure 5, A-1 and B-1). The angular frequency drift of each element is about 2 $|\Omega_{e,eq}|$ rad/s$^2$, which corresponds to ~9 kHz/s at $L^* = 6$ at the equator. Here the drift rate of angular frequency is same as in Section 2. In this study, we assume two repetition periods for whistler elements: 300 msec for simulation A and 100 msec for simulation B. The repetition periods of the element block involving rising tone elements is defined as 3 s. The whistler chorus propagates in the northern and southern directions along the magnetic field with magnetic fluctuation amplitude $|\delta\mathrm{B}| = 100$ pT. The amplitude of electric field fluctuation is calculated from the cold plasma dispersion relation for parallel-propagating whistler mode. Here, we assume that the fluctuation amplitude stays constant, while *Tao et al.* [2012] pointed out the importance of amplitude modulations of chorus elements. Relativistic electrons with equatorial pitch angles less than 10° are distributed at $L^* = 6$. The initial positions of electrons, i.e., the initial equatorial pitch angles, are randomly placed along

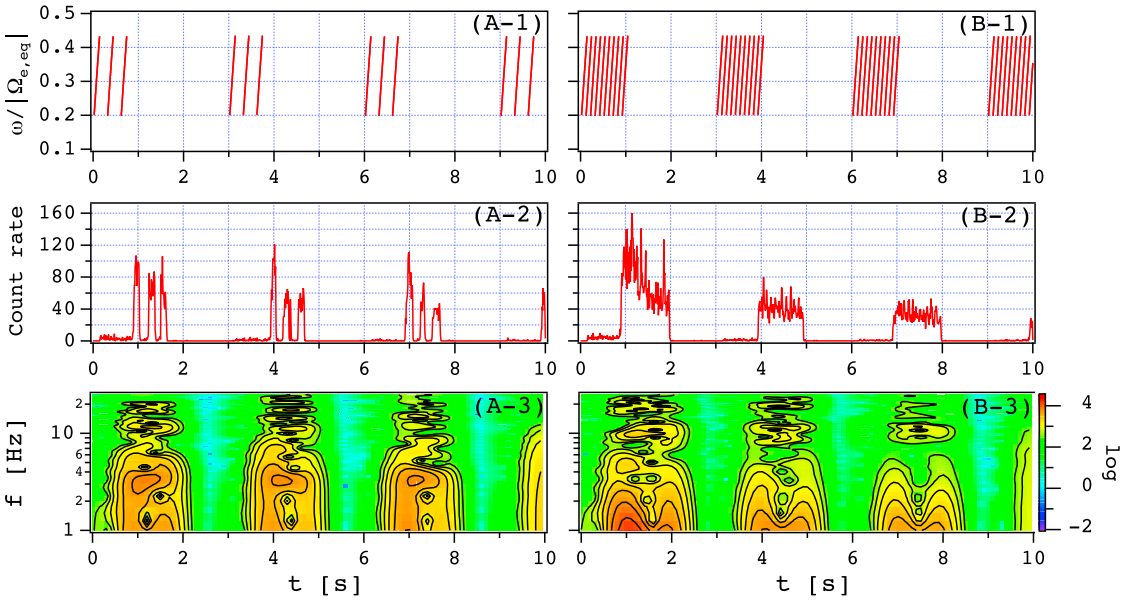


**Figure 5.** (top) Frequency spectra of applied whistler chorus at the equator (labeled by 1), (middle) count rates of precipitated 1 MeV electrons per 10 msec (labeled by 2) at $L^*$ = 6, and (bottom) dynamic frequency spectra of the count rates (labeled by 3) for simulations (left) A and (right) B.

the magnetic field line. Uniform plasma density along the magnetic field line is about 10/cm$^3$, which corresponds to electron plasma frequency $\omega_e \sim 180$ rad/s ($f_e \sim 28$ kHz) which was used in section 2.

## 5. Simulation Results

[20] Figure 5 shows the frequency spectra of the whistler chorus applied at the equator (labeled by 1; top panels), count rates of precipitated 1 MeV electrons per 10 msec (labeled by 2; middle panels) at $L^*$ = 6, and dynamic frequency spectra of the count rates (labeled by 3; bottom panels), for simulations A and B. These count rates of precipitated electrons are sampled at 100 km altitude from the ground: the equatorial loss cone angle is about 2.9°. The whistler chorus emission starts at t = 0 and propagates to higher magnetic latitudes along the dipole field line at $L^*$ = 6. Electrons with energy 1 MeV are scattered through the first-order electron cyclotron resonance at high latitudes. The scattered electrons are observed at the ionospheric altitude (100 km) at about 0.9 sec after the whistler emission and are visible in both simulations, as shown in the middle panels. This delay is explained using the TOF analysis in section 2 (see Figure 1, bottom). In simulation A, the repetition period of the chorus elements is 300 msec (panel A-1), and the precipitation pulses are observed discretely within the 300 msec period (panel A-2). This indicates that the precipitation synchronizes with the whistler chorus emission with a ~0.9 sec delay. The pulse width is about 100 msec, which is the duration of the precipitation related to one whistler chorus element. This duration is also consistent with the relativistic TOF model discussed in section 2. Even with different relativistic energies >500 keV (not shown here), the GEMSIS-RBW simulations show that the delay time and the pulse width are consistent with the relativistic TOF model that considers the propagation of whistler waves along the magnetic field line.

[21] For simulation B, the repetition period of the chorus elements is 100 msec. The short pulse structure of the precipitation seen in simulation A does not appear in simulation B because the duration of the precipitation caused by one whistler chorus element is longer than the repetition period of the whistler chorus emission. The precipitation continues for about 1 s with repetition periods of 3 sec.

[22] The dynamic frequency spectra of the time variations of the count rates shown in Figure 5 (bottom) are plotted using the Gabor transform with a frequency resolution of 1 Hz. For simulation A, the ~3 Hz modulation is identified in each precipitation group. This corresponds to the repeated precipitation pulses with the 300 msec period, as seen in Figure 5 (A-2). The frequency spectrum shows a frequency modulation higher than 3 Hz. We expect that the fluctuations with higher frequencies are associated with the amplitude modulation in shorter time scales than the pulse width (<100 msec).

[23] In simulation B, the fluctuations at relatively broad low frequencies are enhanced around the edges of the precipitation groups. This is associated with the steep edges consisting of continuous Fourier modes. Similar to simulation A, the count rate of the precipitation in simulation B includes a 10 Hz modulation in the panel (B-3), which is associated with the interval between whistler chorus elements. Frequencies higher than 10 Hz are also seen in simulation B, suggesting that the amplitude modulation associated with higher frequencies are included, which is also similar to simulation A.

[24] The frequency spectra of both simulations suggest that whistler chorus emission can modulate the relativistic electron precipitation in frequency related to the chorus emission period. Moreover, the count rates have amplitude modulation with higher frequencies than the chorus emission

frequency (for simulation A: 3 Hz; for simulation B: 10 Hz). We expect that the modulations of the pitch angle distribution near the loss cone edge cause the high frequency modulation. As the number of relativistic electrons near the loss cone edge increases/decreases through the wave-particle interactions, the precipitated electron flux would be modulated in time even if the amplitude of the whistler chorus were constant. The pitch angle of relativistic electrons dynamically changes during the microbursts. Modulation of pitch angle distribution during the scattering by whistler chorus will be the focus of future study.

## 6. Discussion and Summary

[25] We performed a time-of-flight (TOF) analysis of precipitated electrons including relativistic energy range. Results showed that higher-energy electrons are precipitated later in the relativistic regime through the pitch angle scattering by whistler chorus elements at high magnetic latitudes. In contrast, in the non-relativistic regime, lower-energy electrons are precipitated later: that is, the electron precipitation has a negative energy dispersion. We also showed that the duration of relativistic electron precipitation is related to a single whistler chorus element, which is shorter at higher energies. From the relativistic-TOF model, we predict that relativistic electron microbursts will have a positive energy dispersion in the relativistic energy range. If low-altitude satellites observe electron microbursts with a positive energy dispersion, this should be taken as evidence that the whistler chorus propagating to the high magnetic latitudes causes the relativistic electron microbursts.

[26] We confirmed the negative (positive) energy dispersions for low (relativistic) energy ranges. The negative energy dispersion of precipitating electrons is confirmed by a self-consistent particle-in-cell simulation for interactions between whistler chorus waves and electrons [*Hikishima et al.*, 2010], which is consistent with our simulation results. *Miyoshi et al.* [2010] showed that precipitating electrons of ~10 keV have negative dispersions which are well modeled by the TOF model. On the other hand, positive dispersions at relativistic energy have not been identified, and future satellite observations at low altitudes are important to confirm this possibility.

[27] The energy dispersions depend on the plasma density profile along the magnetic field and field line configurations. *Miyoshi et al.* [2010] and *Nishiyama et al.* [2011] developed a method to estimate plasma parameters near the wave-particle interaction regions by comparing the observed energy dispersion and the TOF model with the Tsyganenko magnetic field model [*Tsyganenko and Sitnov*, 2005]. Further simulations with various plasma density profiles as well as realistic magnetic field models, such as the Tsyganenko-model, are necessary for quantitative understanding of characteristics of the energy dispersion of microbursts.

[28] GEMSIS-RBW (RBW) simulations were in agreement with the energy dependent properties derived from the TOF analysis. The simulations also showed the relationship between modulations of the precipitated electrons and the whistler chorus emission; the frequency of the time variations of the count rate (Figure 5, A-3 and B-3) is associated with the interval between whistler chorus elements (Figure 5, A-1 and B-1). Typically, the distribution of intervals between lower band chorus emissions is broad and the related frequency is over a few Hz [e.g., *Trakhtengerts et al.*, 2004; *Santolík et al.*, 2003], so the RBW simulations suggest that the whistler chorus emissions lead to the modulation of relativistic electron microbursts in the broad frequency range. *Nakamura et al.* [1995] conducted a frequency spectrum analysis of microbursts measured by the SAMPEX satellite and identified a broad frequency spectrum over a few Hz. Although they pointed out the relationship between the frequency of fluctuations and the bounce periods of MeV electrons, our simulation identified that the few Hz modulation of the precipitation is a result of wave-particle interactions associated with whistler chorus waves. Our simulation results also revealed modulation of higher frequencies than the repetition frequency of the whistler chorus elements. Note that the count rates for the modulations of the pulse are not so small compared with the total precipitation count rate, so that the high-frequency modulations are real signatures due to the wave-particle interactions. We expect this higher frequency modulation is due to the modulation of the pitch angle distribution near the loss cone edge through nonlinear scattering by whistler chorus.

[29] Our simulation results reproduced a few Hz modulation of the microburst of relativistic electrons measured by the SAMPEX satellite [*Nakamura et al.*, 1995], suggesting that the whistler chorus rising tone propagating to high magnetic latitudes cause the relativistic electron microbursts. We expect that observations with high-time resolutions for the relativistic electrons precipitations at low altitude would provide important clues for understanding of origins of relativistic electron microbursts.

[30] *Nakamura et al.* [1995] also found that many microburst trails show sharp flux increase with more slowly decay. Our simulation results also suggest a signature of the observed property as seen in the first precipitation group of Figure 5 (B-2). Detail analysis of pitch angle distribution during the scattering by whistler chorus may be necessary to understand the observed property of the relativistic electron microbursts, which will be one of important issues in our future works.

[31] It is interesting that the precipitation losses due to microbursts would contribute a part of the flux dropouts of the outer belt. *O'Brien et al.* [2004] suggested that microburst precipitations during the storm main phase are capable of emptying the outer belt in one day or less. On the other hand, chorus waves are important for the non-adiabatic accelerations of relativistic electrons of the outer belt [e.g., *Miyoshi et al.*, 2003; *Horne et al.*, 2005]. The dual roles of chorus waves in the acceleration and precipitation of outer belt electrons will produce various flux variations of the outer belt [*Bortnik and Thorne*, 2007]. Further quantitative estimations by the GEMSIS-RBW simulations are necessary to clarify the balance between the precipitation loss and the accelerations by chorus waves. Effective accelerations are dominantly carried out at ~90 pitch angle around the magnetic equator [e.g., *Omura et al.*, 2007], while electrons near the loss cone edge are lost through the pitch angle scattering by whistler chorus. Thus, in order to demonstrate simultaneously both acceleration and loss, a number of test-particles distributed in whole pitch angle range are required. Moreover, satellite observations of whistler chorus waves are also required to develop more realistic whistler chorus model,

such as wave amplitude, frequency drift rate, emission frequency of chorus elements, spatial distribution of whistler chorus emission, and etc. In future works, the RBW simulations will be done with larger amount of test-particles and more realistic whistler chorus model, and demonstrate flux variation by whistler chorus emissions including both acceleration and loss processes.

## 7. Conclusions

[32] We presented results of test particle simulations to confirm that relativistic electron microbursts can be produced from gyroresonant scattering by whistler chorus elements propagating to high magnetic latitudes. Calculations on time-of-flight model predict timing and energy dispersion of the microbursts, and positive/negative energy dispersions that depend on electron energies are derived. Future observations by the low-altitude satellite that can confirm the energy dispersion of the microburst are essential, which would discriminate whether chorus waves are the origin of the microbursts.

[33] Our test-particle simulation with the wave-particle interaction model (GEMSIS-RBW simulation) confirmed that interactions between chorus waves and relativistic electrons at high latitudes produce microburst precipitations of relativistic electrons of the outer belt. A few Hz modulation in count rates of precipitating electrons that was reported by the SAMPEX observations correspond to the repetition periods of rising tone elements, while it is expected that modulations of higher frequency than the repetition of wave elements are caused by nonlinear wave particle interactions.

[34] **Acknowledgments.** This work was supported by Grant-in-Aid for Scientific Research (B) (20340134, 23340146).

[35] Masaki Fujimoto thanks the reviewers for their assistance in evaluating this paper.

## References

Albert, J. M. (2003), Evaluation of quasi-linear diffusion coefficients for EMIC waves in a multispecies plasma, *J. Geophys. Res.*, *108*(A6), 1249, doi:10.1029/2002JA009792.

Bortnik, J., and R. M. Thorne (2007), The dual role of ELF/VLF chorus waves in the acceleration and precipitation of radiation belt electrons, *J. Atmos. Sol. Terr. Phys.*, *69*, 378–386, doi:10.1016/j.jastp.2006.05.030.

Bortnik, J., R. M. Thorne, T. P. O'Brien, J. C. Green, R. J. Strangeway, Y. Y. Shprits, and D. N. Baker (2006), Observation of two distinct, rapid loss mechanisms during the 20 November 2003 radiation belt dropout event, *J. Geophys. Res.*, *111*, A12216, doi:10.1029/2006JA011802.

Brizard, A. J., and A. A. Chan (1999), Nonlinear relativistic gyrokinetic Vlasov-Maxwell equations, *Phys. Plasmas*, *6*, 4548, doi:10.1063/1.873742.

Ebihara, Y., and Y. Miyoshi (2011), Dynamic inner magnetosphere: A tutorial and recent advances, in *The Dynamic Magnetosphere*, *IAGA Spec. Sopron Book Ser.*, vol. 3, edited by W. Liu and M. Fujimoto, pp. 145–188, Springer, New York, doi:10.1007/978-94-007-0501-2_9.

Furuya, N., Y. Omura, and D. Summers (2008), Relativistic turning acceleration of radiation belt electrons by whistler mode chorus, *J. Geophys. Res.*, *113*, A04224, doi:10.1029/2007JA012478.

Hikishima, M., Y. Omura, and D. Summers (2010), Microburst precipitation of energetic electrons associated with chorus wave generation, *Geophys. Res. Lett.*, *37*, L07103, doi:10.1029/2010GL042678.

Horne, R. B., and R. M. Thorne (2003), Relativistic electron acceleration and precipitation during resonant interactions with whistler-mode chorus, *Geophys. Res. Lett.*, *30*(10), 1527, doi:10.1029/2003GL016973.

Horne, R. B., R. M. Thorne, S. A. Glauert, J. M. Albert, N. P. Meredith, and R. R. Anderson (2005), Timescale for radiation belt electron acceleration by whistler mode chorus waves, *J. Geophys. Res.*, *110*, A03225, doi:10.1029/2004JA010811.

Johnston, W. R., and P. C. Anderson (2010), Storm time occurrence of relativistic electron microbursts in relation to the plasmapause, *J. Geophys. Res.*, *115*, A02205, doi:10.1029/2009JA014328.

Jordanova, V. K., J. Albert, and Y. Miyoshi (2008), Relativistic electron precipitation by EMIC waves from self-consistent global simulations, *J. Geophys. Res.*, *113*, A00A10, doi:10.1029/2008JA013239.

Jordanova, V. K., R. M. Thorne, W. Li, and Y. Miyoshi (2010), Excitation of whistler mode chorus from global ring current simulations, *J. Geophys. Res.*, *115*, A00F10, doi:10.1029/2009JA014810.

Katoh, Y., and Y. Omura (2007), Relativistic particle acceleration in the process of whistler-mode chorus wave generation, *Geophys. Res. Lett.*, *34*, L13102, doi:10.1029/2007GL029758.

Li, W., R. M. Thorne, V. Angelopoulos, J. Bortnik, C. M. Cully, B. Ni, O. LeContel, A. Roux, U. Auster, and W. Magnes (2009), Global distribution of whistler-mode chorus waves observed on the THEMIS spacecraft, *Geophys. Res. Lett.*, *36*, L09104, doi:10.1029/2009GL037595.

Lorentzen, K. R., M. D. Looper, and J. B. Blake (2001a), Relativistic electron microbursts during the GEM storms, *Geophys. Res. Lett.*, *28*, 2573–2576, doi:10.1029/2001GL012926.

Lorentzen, K. R., J. B. Blake, U. S. Inan, and J. Bortnik (2001b), Observations of relativistic electron microbursts in association with VLF chorus, *J. Geophys. Res.*, *106*, 6017–6027, doi:10.1029/2000JA003018.

Millan, R. M., and R. M. Thorne (2007), Review of radiation belt relativistic electron losses, *J. Atmos. Sol. Terr. Phys.*, *69*, 362–377, doi:10.1016/j.jastp.2006.06.019.

Millan, R. M., R. P. Lin, D. M. Smith, K. R. Lorentzen, and M. P. McCarthy (2002), X-ray observations of MeV electron precipitation with a balloon-borne germanium spectrometer, *Geophys. Res. Lett.*, *29*(24), 2194, doi:10.1029/2002GL015922.

Miyoshi, Y., A. Morioka, T. Obara, H. Misawa, T. Nagai, and Y. Kasahara (2003), Rebuilding process of the outer radiation belt during the November 3, 1993, magnetic storm: NOAA and EXOS-D observations, *J. Geophys. Res.*, *108*(A1), 1004, doi:10.1029/2001JA007542.

Miyoshi, Y., K. Sakaguchi, K. Shiokawa, D. Evans, J. Albert, M. Connors, and V. Jordanova (2008), Precipitation of radiation belt electrons by EMIC waves, observed from ground and space, *Geophys. Res. Lett.*, *35*, L23101, doi:10.1029/2008GL035727.

Miyoshi, Y., Y. Katoh, T. Nishiyama, T. Sakanoi, K. Asamura, and M. Hirahara (2010), Time of flight analysis of pulsating aurora electrons, considering wave-particle interactions with propagating whistler mode waves, *J. Geophys. Res.*, *115*, A10312, doi:10.1029/2009JA015127.

Nakamura, R., D. N. Baker, J. B. Blake, S. Kanekal, B. Klecker, and D. Hovestadt (1995), Relativistic electron precipitation enhancements near the outer edge of the radiation belt, *Geophys. Res. Lett.*, *22*, 1129–1132, doi:10.1029/95GL00378.

Nakamura, R., M. Isawa, Y. Kamide, D. N. Baker, J. B. Blake, and M. Looper (2000), SAMPEX observations of precipitation bursts in the outer radiation belt, *J. Geophys. Res.*, *105*, 15,875–15,885, doi:10.1029/2000JA900018.

Nishiyama, N., T. Sakanoi, Y. Miyoshi, Y. Katoh, K. Asamura, S. Okano, and M. Hirahara (2011), The source region and its characteristic of pulsating aurora based on the Reimei observations, *J. Geophys. Res.*, *116*, A03226, doi:10.1029/2010JA015507.

O'Brien, T. P., K. R. Lorentzen, I. R. Mann, N. P. Meredith, J. B. Blake, J. F. Fennell, M. D. Looper, D. K. Milling, and R. R. Anderson (2003), Energization of relativistic electrons in the presence of ULF power and MeV microbursts: Evidence for dual ULF and VLF acceleration, *J. Geophys. Res.*, *108*(A8), 1329, doi:10.1029/2002JA009784.

O'Brien, T. P., M. D. Looper, and J. B. Blake (2004), Quantification of relativistic electron microburst losses during the GEM storms, *Geophys. Res. Lett.*, *31*, L04802, doi:10.1029/2003GL018621.

Omura, Y., N. Furuya, and D. Summers (2007), Relativistic turning acceleration of resonant electrons by coherent whistler mode waves in a dipole magnetic field, *J. Geophys. Res.*, *112*, A06236, doi:10.1029/2006JA012243.

Roederer, J. G. (1970), *Dynamics of Geomagnetically Trapped Radiation*, Springer, Berlin, doi:10.1007/978-3-642-49300-3.

Saito, S., Y. Miyoshi, and K. Seki (2010), A split in the outer radiation belt by magnetopause shadowing: Test particle simulations, *J. Geophys. Res.*, *115*, A08210, doi:10.1029/2009JA014738.

Santolík, O., D. A. Gurnett, J. S. Pickett, M. Parrot, and N. Cornilleau-Wehrlin (2003), Spatio-temporal structure of storm-time chorus, *J. Geophys. Res.*, *108*(A7), 1278, doi:10.1029/2002JA009791.

Summers, D., and R. M. Thorne (2003), Relativistic electron pitch-angle scattering by electromagnetic ion cyclotron waves during geomagnetic storms, *J. Geophys. Res.*, *108*(A4), 1143, doi:10.1029/2002JA009489.

Tao, X., J. Bortnik, R. M. Thorne, J. M. Albert, and W. Li (2012), Effects of amplitude modulation on nonlinear interactions between electrons and chorus waves, *Geophys. Res. Lett.*, *39*, L06102, doi:10.1029/2012GL051202.

Thorne, R. M., and C. F. Kennel (1971), Relativistic electron precipitation during magnetic storm main phase, *J. Geophys. Res.*, *76*(19), 4446–4453, doi:10.1029/JA076i019p04446.

Thorne, R. M., R. B. Horne, S. Glauert, N. P. Meredith, Y. Y. Shprits, D. Summers, and R. Anderson (2005), The influence of wave-particle interactions on relativistic electron dynamics during storms, in *Inner Magnetosphere Interactions: New Perspectives From Imaging*, *Geophys. Monogr. Ser.*, vol. 159, edited by J. Burch, M. Schulz, and H. Spence, pp. 101–112, AGU, Washington, D. C., doi:10.1029/159GM07.

Trakhtengerts, V. Y., A. G. Demekhov, E. E. Titova, B. V. Kozelov, O. Santolik, D. Gurnett, and M. Parrot (2004), Interpretation of Cluster data on chorus emissions using the backward wave oscillator model, *Phys. Plasmas*, *11*, 1345, doi:10.1063/1.1667495.

Tsyganenko, N. A., and M. I. Sitnov (2005), Modeling the dynamics of the inner magnetosphere during strong geomagnetic storms, *J. Geophys. Res.*, *110*, A03208, doi:10.1029/2004JA010798.

Turner, D. L., S. K. Morley, Y. Miyoshi, B. Ni, and C.-L. Huang (2012), Outer radiation belt flux dropouts: Current understanding and unresolved questions, in *Dynamics of the Earth's Radiation Belts and Inner Magnetosphere*, *Geophys. Monogr. Ser.*, AGU, Washington, D. C., in press.

Walt, M. (1994), *Introduction to Geomagnetically Trapped Radiation*, Cambridge Univ. Press, New York, doi:10.1017/CBO9780511524981.